Food Chemistry: X 20 (2023) 100929

Contents lists available at ScienceDirect

Food Chemistry: X

journal homepage: www.sciencedirect.com/journal/food-chemistry-x

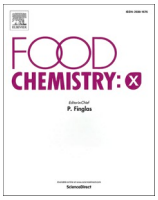

Preparation, structure, and in-vitro hypoglycemic potential of debranched millet starch-fatty acid composite resistant starch

Yunfei Ge [a,b,1], Yu Shi [a,1], Yunjiao Wu [a,1], Chunhong Wei [a,c], LongKui Cao [a,c,*]

[a] College of Food Science, Heilongjiang Bayi Agricultural University, Xinfeng Lu 5, Daqing 163319, China
[b] Department of Marine Food Science and Technology, Gangneung-Wonju National University, 120 Gangneungdaehangno, Gangneung, Gangwon 210-702, Republic of Korea
[c] National Coarse Cereals Engineering Research Center, Heilongjiang Bayi Agricultural University, Daqing 163319, China

ARTICLE INFO

Keywords:
Millet starch
Debranching
Starch-fatty acid complexes
Anti-digestion

ABSTRACT

Currently, the preparation methods and basic physicochemical properties of starch-FA complexes have been widely studied; however, no in-depth research on the regulatory mechanism of the digestive properties of debranched starch-unsaturated FA complexes has been conducted. Therefore, six fatty acids with different carbon chains and different degrees of unsaturation were complexed with de-branched millet starch in this research, using the microwave method. Microwave millet starch-linoleic acid complex (MPS-LOA) had the highest resistant starch (RS) content, and the structure and physicochemical properties of MPS-LOA were determined using various molecular techniques. The results indicate that MPS-LOA had a resistant starch (RS) content of 40.35% and the most notable fluorescence. The characteristic UV peaks of MPS-LOA were blue-shifted, and new IR peaks appeared. The crystalline structure changed to V-type crystals, the crystallinity increased, and the molecular weight decreased. The enthalpy and coagulability of MPS-LOA increased, and the swelling force decreased. Additionally, MPS-LOA showed enhanced α-glucosidase and α-amylase inhibition, and in-vitro hydrolysis kinetics analysis of MPS-LOA showed a hydrolysis index of 53.8 and an extended glycemic index (eGI)I of 54.6, indicating a low eGI food suitable for consumption by people with type II diabetes. These results provide a theoretical basis for the preparation of amylopectin- and starch-based foods with an anti-enzyme structure and a low glycemic index (GI).

Introduction

Millet is among the most important food crops in northern China (Muthamilarasan and Prasad, 2021). Millet contains approximately 56.2–73.1 % starch, and is an important starch source (Punia et al., 2021). In the food industry, millet starch is used as a surfactant, emulsifier, and thickener, and, owing to its medicinal and food values and slow postprandial glycemic rate, be beneficial in the treatment of diseases such as celiac disease and type 2 diabetes (Bangar et al., 2021).

Resistant starch (RS) is a type of starch that is not hydrolyzed by enzymes in the small intestine but can be fermented in the colon to produce short-chain fatty acids such as acetic acid, propionic acid, and butyric acid (Liu et al., 2022). RS can effectively lower the glycemic index (GI), decrease postprandial blood glucose levels, and reduce the risk of developing type II diabetes. RS 5 is a class of resistant starches formed by complexing starch with fatty acids (FAs) (Gutiérrez and Tovar 2021). FAs are embedded in the starch matrix through hydrophobic interactions and hydrogen bonding to form a compact V-shaped complex that increases the enzyme inhibitory power and reduces the postprandial gluconeogenic response. Moreover, RS 5 can be used as wall material for colon-targeted drug delivery systems to prevent diseases such as metabolic syndrome (Kang et al., 2022). In recent years, RS 5 has also been used in other applications, such as carriers for active substances (Liu et al., 2022) and biodegradable, edible packaging films (Kang et al., 2020). Current methods for RS 5 preparation can be categorized as physical, chemical, and enzymatic methods. Physical methods are widely used owing to their environmentally friendly, efficient features. Tao et al. (2020) demonstrated that the microwave dielectric effect leads to the rupture of starch granules, leaching of large amounts of straight-chain and short-chain starch, and the appearance of

* Corresponding author at: College of Food Science, Heilongjiang Bayi Agricultural University, Xinfeng Lu 5, Daqing 163319, China.
E-mail address: caolongkui2013@163.com (L. Cao).
[1] The authors contributed equally to this work.

https://doi.org/10.1016/j.fochx.2023.100929
Received 27 July 2023; Received in revised form 24 September 2023; Accepted 3 October 2023
Available online 11 October 2023

a multiscale structure that is easily bound to the active substance. Chen et al. (2018) prepared lotus seed starch-FA complexes using a microwave method and found that the swelling and radius of gyration of the complexes decreased, the sensitivity of the starch granules to enzymatic digestion decreased, and the content of resistant starch and slowly digested starch increased. Wu et al. (2022) used the microwave-hygrothermal method to prepare corn starch-oleic acid complexes and found that the molecular structure was disrupted and rearranged, forming a highly crystalline V-shaped structure with reduced digestibility. Kang et al. (2022) compared the effects of the ordinary heating method and the microwave method on the complexation rate and crystalline structure of starch-FA complexes and found that the microwave method was more conducive for the formation of starch-FA complexes.

Owing to the high branched chain content in millet starch and its high molecular spatial site resistance, it is difficult to bring complexes into contact with FAs (Liu et al., 2020). Subjecting branched starch to debranching treatment breaks α-1,6-glycosidic bonds, forming medium and short linear starch chains and straight-chain starch, which makes debranched starch highly mobile and free, thus increasing the contact area with FAs and contributing to the formation of more starch-FA complexes. Lee et al. (2021) found that, compared to natural wheat starch, debranched wheat starch has a higher rate of complexation with saturated FAs, forms an indigestible structure that is less susceptible to enzymatic degradation, and inhibits starch retrogradation. Lu et al. (2021) complexed debranched corn starch with saturated FAs of different carbon chains and found that the relative crystallinity of the complexes was increased by 2–3 times and the starch-long-chain FA complexes were more resistant to digestion than other starch-FA complexes prepared under the same conditions. Liu et al. (2020) complexed enzymatically debranched corn starch with lauric acid and found that as the branching density of starch increased, the average chain length and molecular weight decreased, which to some extent promoted the formation of starch-lauric acid complexes and retarded the starch hydrolysis rate.

Therefore, the aim of this study is to investigate the physicochemical properties, in vitro digestibility, and enzyme inhibition of starch-FA complexes. This work will preliminarily explore the regulatory mechanism of the debranched millet starch-linoleic acid complex (MPS-LOA), especially on the "complex structure-digestive properties-in-vitro hypoglycemic potential". In this study, the highest RS content of MPS-LOA will be prepared by microwave method, evaluating how the formation of enzyme-resistant structures and the in-vitro hypoglycemic potential of MPS-LOA, including enzyme inhibition, in vitro-hydrolysis kinetics, and extended glycemic index (eGI). These findings will provide new methods and a theoretical basis for the application of debranched starch-FA complexes of different chain lengths and saturations in the production of novel starch-based functional foods and natural drug development applications.

Materials and methods

Material

The millet was purchased from Xinhao Rice Processing Plant in Luancheng District (Shijiazhuang, China). Pruraminidase (1000 ASPU/g), α-glucosidase (40–80 U/mg), and porcine pancreatic α-amylase (50 U/mg) were purchased from Sigma-Aldrich (Santa Clara, CA, USA). 4-Nitrophenyl-α-D-Glucopyranoside (pNPG), capric acid (CA), lauric acid (LA), palmitic acid (PA), stearic acid (SA), oleic acid (OA), and linoleic acid (LOA) were purchased from Shanghai Aladdin Biochemical Technology Co (Shanghai, China). Acarbose was purchased from Tianxingjian Pharmaceutical Co (Shenyang, China). Soluble starch was purchased from Beihua Fine Chemicals Co (Beijing, China). DNS was prepared in the laboratory of Heilongjiang Bayi Agricultural University (Daqing, China). All other reagents used in the experiments were of analytical grade and purchased from Chemical Company (Tianjin, China).

Preparation of MPS and MPS-FA

The millet was cleaned, dried at 35 °C, and then subjected to dry grinding before being submerged in a 1:3 g/mL solution of NaOH for three hours. This solution was additionally centrifuged for 10 min at 5000 × g to remove the supernatant. The precipitate was then continually rinsed four times and centrifuged till the starch slurry turned white. The pH of slurry was adjusted to 7.0 by 1 mol/L of HCl, then centrifuged, dried at 30 °C, and screened through an 80-mesh sieve, then get the millet starch. (Bangar et al, 2021). Four grams of millet starch were dissolved in 100 mL of distilled water, stirred well, and placed in a microwave oven (M1-L 213C Microwave Oven, Midea Kitchen Appliance Manufacturing Co., Ltd, Wuhu, China) for 90 s at 350 W. The pH was adjusted to 5.5 by 1 mol/L of HCl, cooled to 55 °C, and proalanase was added at 30 U/g millet starch. The mixture was shaken at 55 °C for 16 h to induce debranching, added to a boiling water bath for 10 min to inactivate the enzyme, treated at 4 °C for 24 h, and dried at 40 °C for 24 h to obtain MPS (Van et al., 2012).

Six grams of MPS were dissolved in 100 mL of distilled water and stirred magnetically at 90 °C for 10 min (Solution A); 0.18 g of FAs (capric acid, lauric acid, palmitic acid, stearic acid, oleic acid, LOA) were then added along with 0.2 mL of anhydrous ethanol solution and dissolved in a water bath at 90 °C for 10 min (Solution B). The samples were mixed well and treated in a microwave oven at 700 W for 90 s. Three times the volume of 50 % (v/v) hot ethanol at 60 °C was added and washed by dispersion in a high-speed disperser (FJ- 200S, Sanli Technology Co., Ltd, Shenzhen, China). The sample solution was centrifuged at 5000 × g for 15 min (TDZ 5-WS high-speed centrifuge, Xiang Yi Laboratory Instrument Development Co., Ltd., Hunan, China). The supernatant was then discarded and the above operation was repeated until there was no free oil in the supernatant. Subsequently, the sample was dried at 40 °C for 24 h to obtain MPS-FA. MPS-LOA is a complex of debranched millet starch and LOA.

Hypoglycemic properties of the complex

In- vitro digestibility measurement

We used the method described by Englyst et al. (Englyst and Cummings, 1992) with minor modifications. A total of 0.2 g sample was added to 15 mL of 0.2 mol/L sodium acetate buffer (pH 5.2) and placed in a boiling water bath for 20 min. Subsequently, 8 glass beads were added to the sample and placed in a water bath at 37 °C and shaken for 10 min, after which 5 mL of mixed enzyme solution (Enzyme solution preparation: porcine pancreatic α-amylase 300 U/mL, amyloglucosidase 50 U/mL) was added. The shaker was maintained at 37 °C and 110 r/min. After adding 4.5 mL of anhydrous ethanol to 0.5 mL of the supernatant at 20, 40, 60, 80, 100, 120, and 180 min, 1 mL of the solution was taken to which 1 mL of distilled water and 1.5 mL of DNS solution were added, boiled for 5 min, cooled to room temperature of 25 °C and made up to 10 mL, and the absorbance at 540 nm was measured. Each experiment was repeated three times.

$$\mathrm{RDS} = (\mathrm{G}\,20 - \mathrm{G}0) \times 0.9 \times 100/\mathrm{TS}$$

$$\mathrm{SDS} = (\mathrm{G}\,120 - \mathrm{G}\,20) \times 0.9 \times 100/\mathrm{TS}$$

$$\mathrm{RS} = (100 - \mathrm{RDS} - \mathrm{SDS})$$

where TS is the total starch content in the sample (mg) and G 20 and G 120 are the glucose contents after 20 min and 120 min of amylase hydrolysis (mg), respectively, and 0.9 is the conversion factor, RDS is the fast-digesting starch (%) and SDS is the slow-digesting starch (%), RS is the resistant starch (%).

Measurement of enzyme activity inhibition

(1) α-glucosidase activity assay

We used the method described by Wang et al. (2019) with minor modifications; 100 μL of α-glucosidase solution (10 U/mL) was pipetted and incubated at 37 °C for 10 min, and 50 μL of sample solutions of different concentrations and 50 μL of pNPG solution (5 mmol/L) were added and incubated at 37 °C for 35 min, after which 50 μL of Na2CO3 solution (0.2 mol/L) was added to terminate the enzymatic digestion. The absorbance at 405 nm was measured using a SPECTROstarNano enzyme standardization instrument (BMG LABTECH GmbH, Germany). Acarbose was used as a positive control, and the enzyme activity inhibition rate was calculated.

$$\text{Enzyme activity inhibition rate} = \left(1 - \frac{A_1 - A_2}{A_3 - A_0}\right) \times 100\%$$

where A1 is the absorbance when the sample solution and enzyme solution are added; A2 is the absorbance when the sample solution is added and enzyme solution is not added; A3 is the absorbance when the enzyme solution is added and sample solution is not added; and A0 is the absorbance when the sample solution and enzyme solution are not added.

(2) α-amylase activity assay

We used the method described by Yadav et al. (2021) with minor modifications; 40 μL of sample solutions of different concentrations were incubated with 40 μL of porcine pancreatic α-amylase (10 U/mL) at 37 ℃ for 30 min. The sample was incubated for 10 min after adding 40 μL of soluble starch (1 g/100 mL), and 160 μLDNS was added and boiled for 5 min for color development. Two times the volume of distilled water was then added for dilution. The absorbance at 405 nm was measured using a SPECTROstar Nano enzyme standardization instrument (BMG LABTECH GmbH, Germany). Acarbose was used as a positive control, and the enzyme activity inhibition rate was calculated.

$$\text{Enzyme activity inhibition rate} = \left(1 - \frac{A_1 - A_2}{A_3 - A_0}\right) \times 100\%$$

where A1 is the absorbance when the sample solution and enzyme solution are added; A2 is the absorbance when the sample solution is added and enzyme solution is not added; A3 is the absorbance when the enzyme solution is added and sample solution is not added; A0 is the absorbance when the sample solution and enzyme solution are not added.

In-vitro hydrolysis kinetics and eGI measurement

The glucose content of the samples at different time points was determined using the method of Englyst and Cummings (1992). The starch hydrolysis rate and time were plotted and fitted with first-order kinetics, and the estimated glycemic index was determined according to the method of Granfeldt et al. (1994).

$$C = \left(1 - e^{-kt}\right)C_\infty$$

$$AUC = C_\infty(t - t_0) - \frac{C_\infty}{k}\left[1 - \exp^{-k(t-t_0)}\right]$$

$$HI\% = \frac{AUC_{sample}}{AUC_{Standard\ Products}} \times 100\%$$

$$eGI = 8.198 + 0.862HI$$

where C is the sample hydrolysis rate at time t; C∞ is the sample hydrolysis rate at equilibrium; k is the digestion kinetic constant; AUC is the area of the hydrolysis curve; HI is the hydrolysis index; and eGI is the predicted glycemic index.

Physicochemical properties of the complexes

Thermal characteristics measurement

A 3 mg sample was placed in an aluminum disc crucible, 9 μL of deionized water was added, and stored at 4 °C for 12 h to equilibrate the moisture. Thermal characteristic measurements were performed using differential scanning calorimetry (DSC; DSC25, TA Instruments, USA) with the following parameters: heating rate of 10 °C/min, temperature range of 20–140 °C, and nitrogen flow rate of 20 mL/min (Raza et al., 2021).

Swelling capacity measurement

One gram of sample was placed in a 100 mL centrifuge tube and 50 mL of distilled water was added, mixed well, shaken in a water bath at 90 °C for 30 min periodically on the VORTEX 3 vortex shaker (IKA Instruments GmbH, Germany), cooled to room temperature of 25 °C, and centrifuged at 4500 rpm for 15 min. The supernatant was poured into an aluminum box and dried at 105 °C to a constant weight (Oskaybas-Emlek et al., 2022). Each experiment was repeated three times.

The swelling capacity measurement was calculated as follows:

$$S = \frac{m_1}{1.0} \times 100\%$$

$$SP = \frac{m_2}{1.0 \times (1 - S\%)}$$

where S is the solubility (%), SP is the swelling power (g/g), m1 is the mass of the supernatant (g), and m2 is the mass of the precipitate in the centrifuge tube (g).

Coagulability measurement

One gram of sample was dispersed in 100 mL of distilled water, boiled in a water bath for 30 min, and then cooled to room temperature. The sample was refrigerated at 4 °C for 4 days, its transmittance was measured at 650 nm every 24 h, and the volume of precipitates was recorded. The blank control group was replaced with distilled water (Cervantes-Ramirez et al., 2020). Each experiment was repeated three times.

Structural analysis of the complexes

Fat content measurement

(1) Free fat

Two and a half grams of sample were taken in a cellulose cartridge and transferred to a Soxhlet extractor. Petroleum ether was then added and Soxhlet extraction was performed at 55 °C for 10 h. After repeated reflux, the collection bottle containing the fat was dried in an oven at 105 °C to a constant weight (Cai et al., 2022). Each experiment was repeated three times.

$$F = \frac{m_2 - m_1}{2.5} \times 100$$

where F is the free fat content (%), m1 is the mass of the fat and collection bottle after drying (g), and m2 is the mass of the collection bottle before drying (g).

(2) Total fat

Two grams of the sample were taken and added to 20 mL of distilled water and 30 mL of 8 mol/L HCl, placed in a boiling water bath for 25 min. Subsequently, 50 mL of distilled water was added and the sample was washed until neutral pH was achieved, and oven-dried at 40 °C for

10 h. The Soxhlet extraction method described in 2.4.1 was used, and the total fat content of each sample was calculated and repeated three times (Raza et al., 2021).

(3) Complex fat content

The complex fat content was calculated as follows:

$$C = T - F$$

where C is the compound fat content (%), T is the total fat (%), and F is the free fat content (%).

Fluorescence microscopy

Twenty milligrams of the sample were added to 1 mL of 1 mg/mL Nile Red staining solution. The precipitate was stained at 4 °C for 24 h and centrifuged at 5000 rpm for 30 min. The supernatant was removed, 1.5 mL of anhydrous methanol was added, and the mixture was centrifuged at 5000 r/min for 15 min. This was repeated to wash off the excess dye. Sample was pipetted onto a clean slide, one drop of anhydrous methanol was added, a coverslip was placed, and air bubbles were removed and observed using an *ortho*-fluorescence microscope (Nikon Eclipse Ci, Nikon Corporation, Japan) under a red filter (Cai et al., 2022).

Iodine adsorption capacity measurement

A 0.2 g sample was added to 10 mL DMSO solution and boiled in a water bath for 20 min. Concurrently, 10 mL of starch emulsion was added to 30 mL of deionized water. The pH was adjusted to 3 with 2 mol/L HCl, and 0.5 mL of iodine solution (2 % KI, 0.2 % I2) was added; the volume was made up to 100 mL and left to stand for 30 min away from light, and the iodine adsorption capacity was measured using a UV–visible spectrophotometer (T6, Pulyanalysis General Instrument Co., Ltd., Beijing, China) in the wavelength range of 400 ~ 800 nm (Krishnan et al., 2020).

Functional group determination

Ten milligrams of the sample were mixed with KBr powder in the ratio of 1:100, ground, mixed, pressed into a tablet, and scanned using a Fourier-transform infrared spectrometer (Nicolet 6700, Thermo Nicolet Corporation, Madion, WI, USA) (Xu et al. 2019).

Crystalline structure determination

The samples were uniformly dispersed flat in the operation frame and measured using X-ray diffractometer (D 8 ADVANCE, Bruker Corporation, Germany) with the following parameters: tube current 40 mA, tube voltage 40 kV, Cu target wavelength 1.5406 Å, scanning angle range 3–60 ° (2 θ), and scanning rate 5 (°)/min (Li et al., 2021).

Nuclear magnetic resonance (NMR) carbon spectroscopy

NMR spectra were determined according to the method described by Tan et al. (2007). The sample was dissolved in D2O and measured using a 600 MHZ NMR (AVANCE III 600 M, Bruker Corporation, Germany).

Absolute molecular weight measurement

Five milligrams of the sample were weighed, added to 5 mL DMSO solution, and dissolved by heating at 80 °C for 3 h. Subsequently, 200 μL of the sample was aspirated and used to determine the absolute molecular weight measurement by gel permeation chromatography (GPC-20A, Shimadzu Corporation, Japan). The column temperature was 60 °C; the mobile phase was 0.5 % LiBr, DMSO; flow rate was 0.3 mL/min; and elution gradient was isocratic 120 min (Kang et al., 2022).

Statistical analysis

All trials were set up in at least three parallel groups, and data were expressed as mean ± standard deviation and analyzed by analysis of variance using SPSS Statistics 25 (IBM SPSS Statistics 25.0, IBM, Armonk, NY, USA). Statistical significance was set at $P < 0.05$. All graphs were plotted using Origin software (OriginPro 2019b, MicroCal, Northampton, MA, USA) based on the experimental data.

Results and discussion

Digestive and hypoglycemic properties analysis

(1) In- vitro digestibility analysis

Fig. 1(a) shows the distribution of the RDS, SDS, and RS contents of MPS with different MPS-FA complexes. Compared with MPS, the RS and SDS contents of all six MPS-FA complexes increased to different degrees, while the RDS contents decreased, with MPS-LOA exhibiting the most notable decreasing trend at 64.92 %, which was likely the result of the FAs being embedded on the outer surface of the starch granules due to hydrogen bonding during the preparation process, thus reducing the potential binding sites for digestive enzymes, and with the partial conversion of RDS to RS with SDS (Li et al., 2021). Comparing the in-vitro digestibility of the six MPS-FA complexes, the RDS of the complexes decreased with the number of FA carbon chains and the RS increased with the number of FA carbon chains. When the number of FA carbon chains remained constant, the LOA complex with unsaturation degree two was more resistant to digestion than the oleic acid complex with unsaturation degree one. The highest RS content of 40.35 % was obtained in the MPS-LOA complex, indicating that the MPS-LOA complex had the best resistance to digestion. The hydrophobicity of FAs gradually increases as chain length increases, and the intermolecular forces between the two molecules are strengthened when complexation with starch occurs, which to some extent increases the structural stability of the complex and improves its indigestibility (Sun et al., 2021). Therefore, a subsequent study was conducted using MPS-LOA to further analyze the molecular mechanism of LOA in enhancing the enzymatic resistance of debranched starch.

(2) The enzyme activity inhibition analysis

The inhibition rates of α-glucosidase and cα-amylase by MPS and MPS-LOA are shown in Fig. 1(b-c), which is beneficial for reducing postprandial blood glucose (Wang et al., 2019) As shown in the figure, both MPS and MPS-LOA inhibited both digestive enzymes, with α-amylase inhibition being significantly stronger than that of α-glucosidase and lower than that of the positive control acarbose. MPS-LOA had IC 50 values of 25.98 mg/mL and 1.13 mg/mL for α-glucosidase and α-amylase, respectively. As the concentration increased, the enzyme inhibitory capacity increased and then leveled off, showing a dose-dependent relationship; however, at the same concentration as MPS-LOA, MPS showed weaker inhibition of the enzyme. And the presence of LOA causes MPS-LOA to inhibit enzymes more effectively than MPS (Sangilimuthu et al., 2021, Dang et al., 2016). It is possible that the enzymatic inhibition of MPS-LOA is elevated because of its low molecular weight and highly dense structural features that block enzymatic digestion and affect the active site of the enzyme (Li et al., 2021). Meanwhile, LOA belongs to a class of long-chain FAs containing two unsaturated double bonds with a large spatial site resistance that can prevent hydrolysis by enzymes (Raza et al., 2021).

(3) In-vitro hydrolysis kinetics and eGI measurement analysis

Fig. 1(d-e) shows the in-vitro hydrolysis curves, in-vitro hydrolysis kinetics, and HI and eGI values of MPS with MPS-LOA. As shown in Fig. 1(d), the hydrolysis rates of MPS and MPS-LOA were faster in the first 20 min, and then slowly increased until they stabilized, reaching a plateau at 37 min, and MPS-LOA hydrolysis reached a plateau at 58 min.

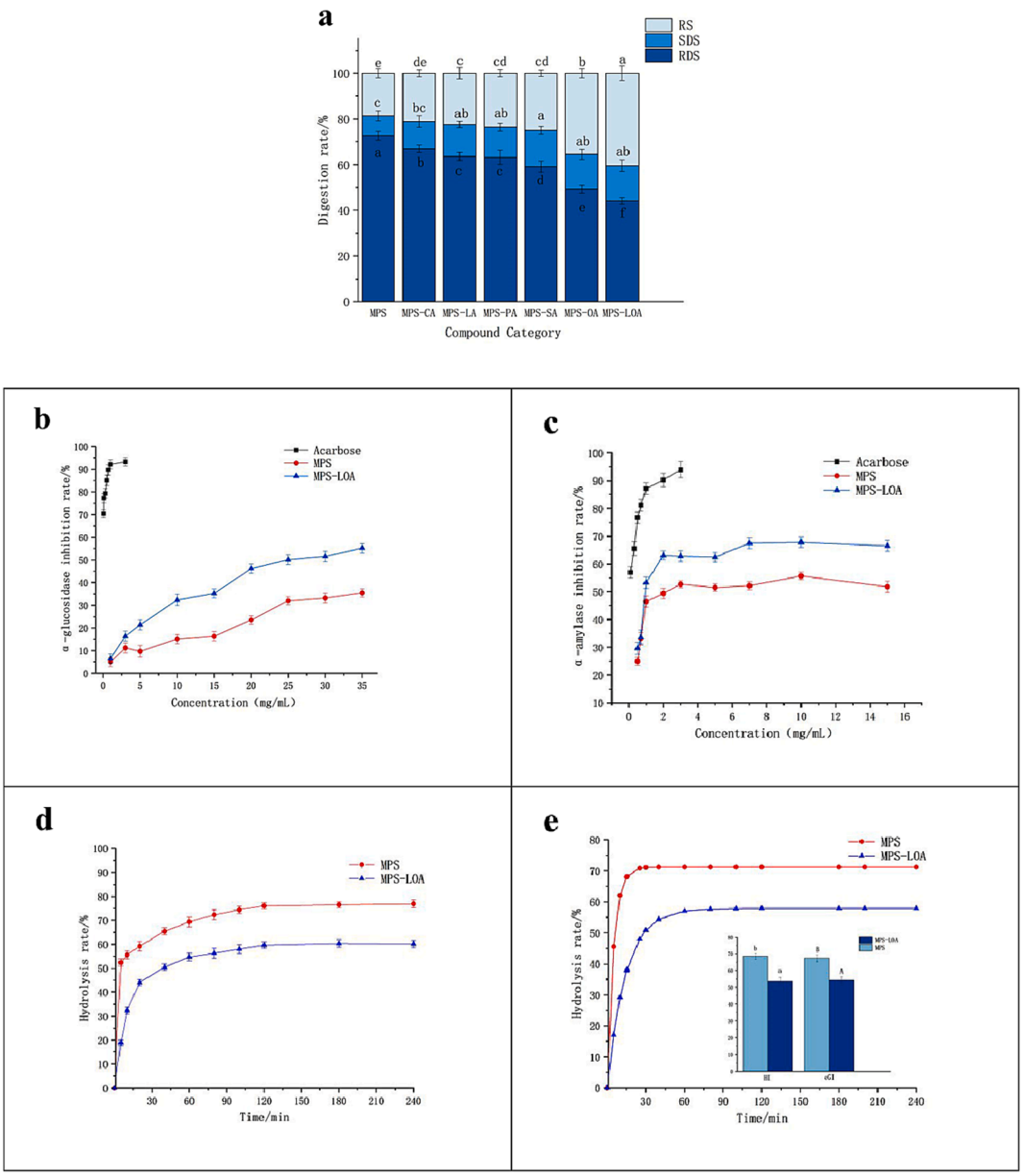

Fig. 1. Digestive and hypoglycemic properties analysis. (a) In vitro digestibility of MPS and MPS-FA. Different superscript letters on the bar graph indicate significant differences ($P < 0.05$). MPA is debranched millet starch; MPS-CA is debranched millet starch-decanoic acid complex; MPS-LA is debranched millet starch-lauric acid complex; MPS-PA is debranched millet starch-palmitic acid complex; MPS-SA is debranched millet starch-stearic acid complex. MPS-OA is a debranched millet starch-oleic acid complex; MPS-LOA is a debranched millet starch-linoleic acid complex. (b) Inhibition of α-glucosidase by MPS and MPS-LOA. (c) Inhibition of α-amylase by MPS and MPS-LOA. (d) Hydrolysis curves of MPS with MPS-LOA. (e) In -vitro hydrolysis kinetics and their eGI values.

Compared to MPS, the final digestibility of MPS-LOA was 57.8 %, representing a decrease of 18.8 %, indicating that MPS-LOA had better digestibility resistance and stability. The strong thermal effect of microwaves can lead to the disruption of the starch helical structure and deconvolution, producing a large number of medium- and short-chain starch fragments, thereby facilitating the complexation of the LOA tail with the hydrophobic cavity of the straight-chain starch, and the contact of the carboxyl group with the polar molecules to recrystallize and form a more thermally stable type II structure (Cervantes-Ramirez et al., 2020), which is consistent with the DSC results of this study. Additionally, MPS complexed with LOA forms a V-complex, which increases the stacking density of the starch structure, making it less sensitive to hydrolytic enzymes and reducing the availability of active sites (Raza et al., 2021), resulting in slow digestion. Wu et al. (2022) used a microwave-hygrothermal method to prepare corn starch-oleic acid complexes and found that the helical structure of starch was separated, the molecular arrangement was disrupted, and microwave-hygrothermal treatment caused the rearrangement of starch and oleic acid to form a highly crystalline V-shaped crystal structure with a decreased hydrolysis rate and increased resistance to enzymes.

Foods can be classified as high eGI (eGI > 70), medium eGI (70 > eGI > 55), or low eGI (eGI < 55) based on their postprandial glucose production capacity (Jenkins et al., 1981). As shown in Fig. 1(e), the eGI of MPS was 67.1, and the eGI of MPS-LOA was 54.6, indicating that MPS-LOA is a low eGI food capable of delaying gluconeogenesis.

(4) Swelling capacity and coagulability analysis

As shown in Table S1, the addition of LOA had a substantial effect on the swelling capacity of starch. The solubility and swelling of MPS-LOA

were significantly lower than those of MPS ($P < 0.05$). This may be due to the microwave leading to the fragmentation of starch granules, where LOA can be embedded in the lamellar structure and form a hydrophobic film on the surface of MPS with reduced hydration (Kang et al., 2020). Alternatively, it may be due to the rearrangement of the damaged starch molecular chains. During the recrystallization process, LOA and MPS form a new, dense structure, which hinders the entry of water molecules (Oskaybas-Emlek et al., 2022), resulting in reduced swelling capacity. Furthermore, Mapengo et al. (Mapengo et al., 2021) prepared maize starch-stearic acid complexes and discovered that changes in the starch structure could affect the swelling power of the complexes, as well as their resistance and slow digestibility. The light transmission and sink volume of the MPS-LOA were lower than those of MPS. During microwave preparation, the helical structure of starch is severely disrupted by the high energy generated by microwaves, and LOA recrystallizes in the starch helical cavity through hydrophobic forces to form new aggregates (Oskaybas-Emlek et al., 2022), which hinders light transmission and weakens the binding force with water, thereby improving the coagulation stability and digestibility resistance of MPS-LOA.

Fat distribution analysis

Fig. 2 shows the fluorescence microscopy results for MPS and MPS-LOA. As shown in the figure, MPS showed a weak red fluorescence, but MPS-LOA was stained, and the red color appeared uniformly throughout the matrix and emitted a very strong fluorescence, as shown in the white circle area in Fig. 2. The fluorescent coloration of MPS may be caused by severe physical and debranching damage to the granule structure, including cracks, pores and other apparent morphology (Wu et al., 2022, Lee et al., 2021), and the Nile Red reagent may be physically trapped in the structural gaps of the starch such that it cannot be washed easily by methanol (Tao et al., 2020). Alternatively, it may be caused by the presence of minute quantities of endogenous lipids still present in MPS (Cai et al., 2022). Table 1 shows the percentage of lipid content in MPS and MPS-LOA. Compared with MPS, the free fat, total fat, and complex fat contents of MPS-LOA were significantly increased, among which the free fat and complex fat contents increased to 0.74 % and 1.05 %, respectively, and indicating that the microwave method can effectively complex starch and FAs, which is conducive to MPS-LOA formation (Tao et al., 2020). Kang et al. (2022) analyzed two types of wheat starch-FA complexes prepared using the water bath and microwave methods in terms of comparative macrostructure and microstructure, and found that the microwave process resulted in the formation of more easily complexed starch structures with FAs. Additionally, Guo et al. (2021) showed that the unsaturated double bond of LOA leads to the bending of FA carbon chains, and the bent carbon chain structure is more favorable for MPS-LOA formation. The red fluorescence of MPS-LOA compared to MPS indicates that MPS-LOA is rich in FAs, and this FA fraction may consist of three FAs that are trapped within the starch granule cleavage layer (Cai et al., 2022), adsorbed on the surface of the starch granule, and encapsulated inside the starch granule as an inner core material (Zhang et al., 2022). Jia et al. (2018) found that the lotus seed starch-FA complexes exhibited bright red spots compared to lotus seed starch, which was attributed to the presence of FA crystals between the lamellar structures of the lotus seed starch, in agreement with the results of this study.

Table 1
Lipid contents of MPS and MPS-LOA.

Sample	F/%	T/%	C/%
MPS	0.57 ± 0.01^{b}	0.78 ± 0.04^{b}	0.21 ± 0.03^{b}
MPS-LOA	0.74 ± 0.06^{a}	1.79 ± 0.04^{a}	1.05 ± 0.02^{a}

Note: Values in the table are mean ± standard deviation. Different subscript letters within the same column indicate significant differences ($p < 0.05$). In Table 1, MPA is debranched millet starch; MPS-LOA is debranched millet starch-linoleic acid complex.

Helical structure analysis

(1) UV spectra of MPS and MPS-LOA analysis

Fig. 3(a) shows the full-wavelength scanning spectra of iodine adsorption on MPS with MPS-LOA. As shown in the figure, the maximum absorbance of MPS was near 600 nm, and the maximum absorbance of MPS-LOA was near 550 nm. Compared with MPS, the characteristic peak of MPS-LOA shifts to a lower wavelength and shows a decreasing trend in absorbance with a color reduction effect (Wang et al., 2010)., indicating that the presence of LOA inhibits the formation of starch-iodine complexes (Krishnan et al., 2020). Some of the LOA may enter the helical structure due to hydrophobic interactions, forming a compact and ordered structure that is not easily complexed with iodine, leading to a decrease in absorbance (Liu et al., 2009).

(2) Fourier-Transform Infrared (FTIR) spectra of MPS and MPA-LOA analysis

The Fourier-transform infrared spectra of MPS and MPS-LOA are shown in Fig. 3(b). Compared with MPS, the peak near 3400 cm-1 shifted to a lower wavenumber and a red-shifted phenomenon occurred, indicating that hydrogen bonding increased and –OH became more stable, while some starch and FAs could have been bound by hydrogen bonding (Govindaraju et al., 2022). Chumsri et al. (2022) found that the rice starch-FA complexes underwent a peak shift at 3300 cm-1 with enhanced –OH stability, increased hydrogen bonding, and increased resistant starch content. MPS-LOA showed two new characteristic peaks at 2853 cm^{-1} and 1740 cm^{-1}. The peak at 2853 cm^{-1} caused by the asymmetric stretching vibration of FAs –CH2 and –CH3 in the single

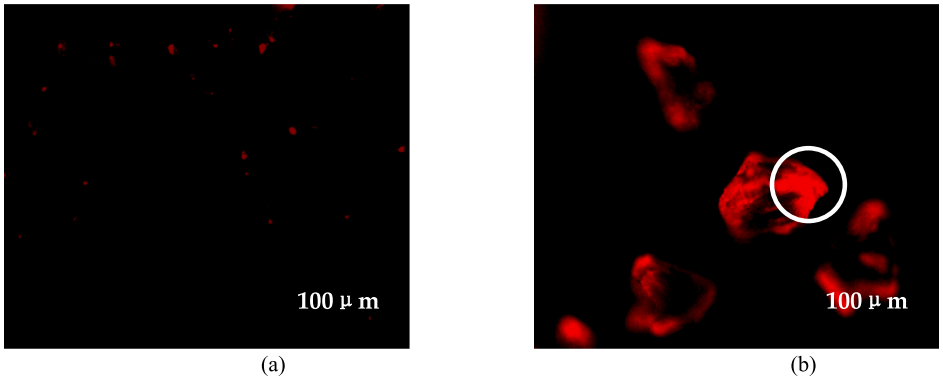

(a) (b)

Fig. 2. Fluorescence microscope images of MPS and MPS-LOA. (a) MPS; (b) MPS-LOA.

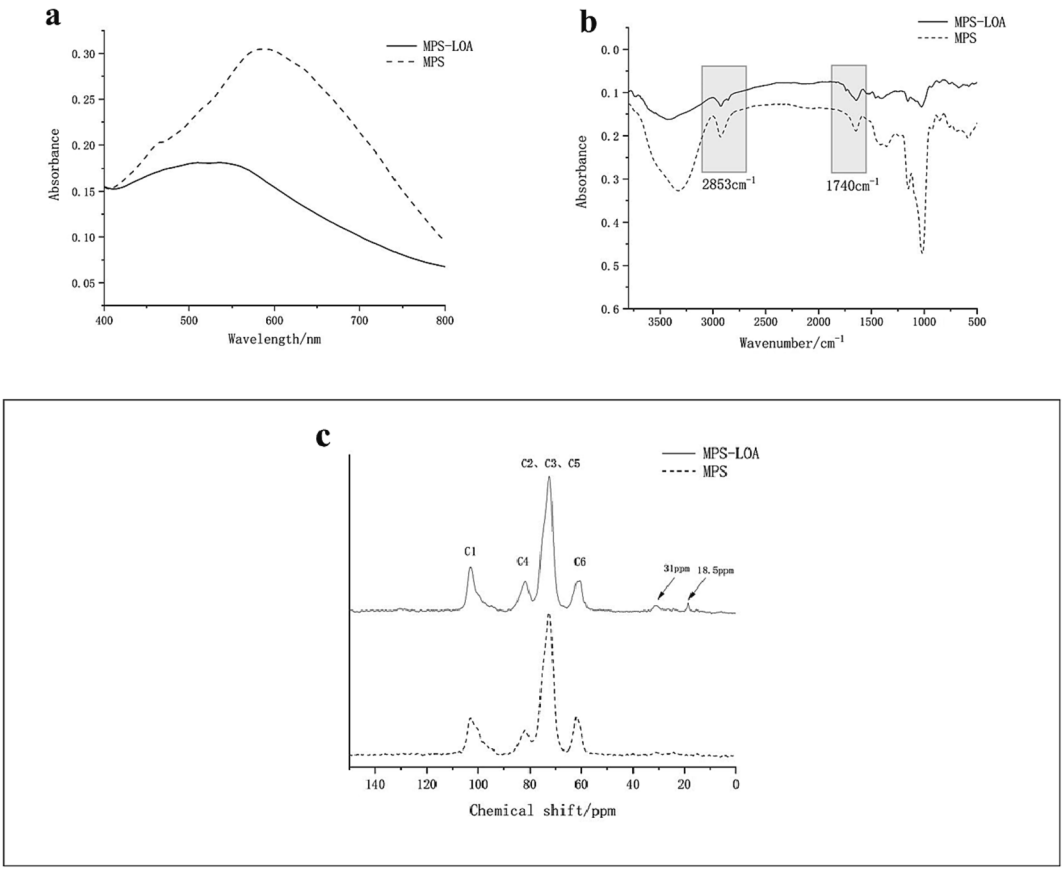

Fig. 3. Helical structure analysis. (a) UV spectra of MPS and MPS-LOA. (b) Fourier-Transform Infrared (FTIR) spectra of MPS and MPA-LOA. (c) NMR 13C spectra of MPS and MPS-LOA.

helix structure of starch (Lu et al., 2021, Oskaybas-Emlek et al., 2022) and that at 1740 cm^{-1} caused by –C═O stretching vibration also verified the complexation of MPS with LOA in the reaction system to form MPS-LOA (Liu et al., 2022). Li et al. (2019) used Fourier-transform infrared spectroscopy to study the structural characteristics of yam starch-palmitic acid complexes. They found that two additional peaks appeared at 2846 cm^{-1} and 1705 cm^{-1}, which were attributed to the deconvolution of starch during the preparation process and the breakage of hydrogen bonds between the carboxyl groups of palmitic acid and the entry of palmitic acid into the starch structure. At the same time, the two new characteristic peaks also appeared in the starch-FA complex prepared by Guo et al. (2021). Therefore, the result also verified the formation of MPS-LOA. The structural properties of the amorphous area of starch are represented by the infrared absorption at 1022 cm^{-1}, and those of the crystalline portion of the starch molecules are represented by the infrared absorption at 1047 cm^{-1} (Millan-Testa et al., 2005). The figure shows that the sensitivities of MPS and MPS-LOA in the crystalline and amorphous regions are different from one another, indicating that the crystal structure of MPS-LOA synthesized by the microwave approach has changed in comparison to MPS. The X-ray diffraction pattern provided further support for this finding.

(3) NMR 13C spectra of MPS and MPS-LOA analysis

Fig. 3(c) shows the 13C CP/MAS NMR spectra of MPS and MPS-LOA. Compared to MPS, MPS-LOA underwent a chemical shift upward at 31.5 $\times 10^{-6}$ and 18.5 $\times 10^{-6}$, while MPS did not show resonance and the single helix structure diffraction peaks became sharper with increased peak intensity, which was attributed to the formation of the MPS-LOA complex with C and COOH resonance (Zheng et al., 2020) on the hydrophobic bond of LOA (Wu et al., 2022). Yan et al. (2020) used a hydrothermal method to prepare corn starch-saturated FA complexes, which also showed FA resonance peaks in the range of 31–32 $\times 10^{-6}$. Table S2 shows the chemical shifts and helical structure distributions of the MPS and MPS-LOA. From the table, the C1 chemical shifts of MPS were 102.6 $\times 10^{-6}$ and 100.1 $\times 10^{-6}$, and the C4 chemical shift was 81.8 $\times 10^{-6}$, which belonged to the B-type crystal. The C1 chemical shift of MPS-LOA was 103.2 $\times 10^{-6}$ and the C4 chemical shift was 81.7 $\times 10^{-6}$, which belonged to the V6-type crystal. In NMR carbon spectroscopy analysis, the crystallinity and helical structure of starch affected the chemical shifts of C1 and C4 (Sun et al., 2021). The complexes of MPS with LOA can be determined from the chemical shifts of C1 and C4 in MPS-LOA as V6 type I and V6 type III crystal structures among V6 type crystals. V6 type I indicates that the FAs are all present in the hydrophobic cavities of starch, and V6 type II and V6 type III indicate that the FAs can also be present in the gaps of starch granules (Jia et al., 2018, Le-Bail et al., 2015). This indicates that the presence of LOA in MPS-LOA is different. The FA content and fluorescence micrographs obtained in this study also indicate that LOA is present in MPS-LOA in a variety of forms. Sun et al. (2021) used solid-state NMR to study the structural characterization of maize starch-FA complexes. They found that the C1 signal of the complexes conformed to the typical features of V6-type structure. In addition, compared to MPS, MPS-LOA shows a single peak and increased chemical shift at C1, but the chemical shifts of C4 and C6 are reduced by 0.1 $\times 10^{-6}$ and 0.4 $\times 10^{-6}$, respectively, due to the chemical bond torsion angle conversion during the complexation of MPS and LOA in forming a new helical structure, which also indicates a higher degree of helicity and a more stable structure of MPS-LOA (Le-Bail et al., 2015). Compared with MPS, the double helix content and FWHM of MPS-LOA decreased and the single helix content and PPA increased, indicating that during microwave preparation, the original double helix structure of starch was destroyed and deconvoluted, a large number of medium

and short-chain starch fragments were dissolved, and the amorphous region increased. Under the hydrophobic effect, LOA is forced to combine with fragmented chains in the amorphous region (Tan et al., 2007) and enter the helical cavity formed by straight-chain starch, which is transformed into a highly structurally ordered and uniformly distributed single (Wu et al., 2022). It has also been shown that because MPS-LOA has an ordered and stable polycrystalline structure, it can enhance its resistance to enzymatic hydrolysis (Sun et al., 2021), resulting in a higher RS content and increased digestibility of MPS-LOA. This result is consistent with the results of the in vitro digestibility analysis.

Crystal structure analysis

Fig. 4 shows the results of the X-ray diffraction (XRD) analysis of the MPS and MPS-LOA. As shown in the figure, the diffraction angle corresponding to the MPS diffraction peak appears as a single peak near 17° and 19°, indicating that the de-branched starch MPS is a typical B-type structure (Lu et al., 2021). Compared with MPS, the diffraction angles 17° and 19° merge to form new broad diffraction peaks after the addition of LOA, and the characteristic diffraction peaks of stronger V-shaped crystal structures appear around 7.4°, 12.9°, and 19.8°, and the crystal shape changes from B-type to V-type, indicating an interaction between MPS and LOA that results in their complexation (Tan et al., 2007). Therefore, XRD indicates that MPS-LOA is a Va crystal structure. Furthermore, the crystallinity of MPS-LOA was substantially improved compared to that of MPS (10.67 %), which was 17.95 %. The transformation of the crystal structure and the improvement of the crystallinity were analyzed because the double helix structure of starch is opened during the microwave treatment (Ma et al., 2018), the natural semi-crystalline structure is destroyed, short-chain molecules are fully released (Wu et al., 2022) to form a hydrophobic cavity composed of the outer hydroxyl hydrophilic group, and the inner methylene and glycosidic oxygen atoms and the non-polar part of LOA entered the cavity of starch to form a new structure owing to hydrophobic forces (Li et al., 2021). Raza et al. (2021) used ultrasonication to prepare the tsukemono starch-LOA complex and found that the crystalline shape changed to highly crystalline V-shaped crystals, which is consistent with the results of this experiment. Xu et al. (2019) showed that there exists a relationship between the crystalline properties of starch and its digestibility resistance, and that the formation of V-shaped crystals with high crystallinity gives MPS-LOA a dense and stable structure with strong digestibility resistance.

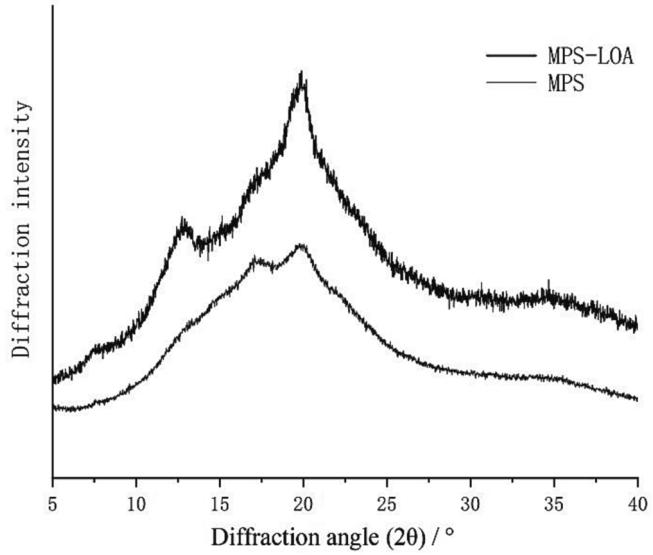

Fig. 4. X-ray diffraction (XRD) pattern of MPS and MPS-LOA.

TO, TP, TC, ΔH, and TC-TO, reflecting the changes in the thermodynamic properties of the MPS and MPS-LOA, are presented in Table S3. As shown in Table S3, the TP of MPS was 90.3 °C and that of MPS-LOA was 118.3 °C, indicating that MPS formed a type I disordered crystal structure and MPS-LOA formed a type II stable crystal structure (Oyeyinka et al., 2021). Huang et al. (2021) prepared corn starch-lauric acid complexes using a water bath method and found that the complexes were also type II starch-FA complexes that had good thermal stability and were not easily destroyed during thermal processing. Compared with MPS, the TO, TP, and TC of MPS-LOA moved toward higher temperatures, TC-TO decreased, and the heat absorption peak became narrow and sharp. The amorphous region of starch increased during microwave treatment, and FAs entered the single helix cavity of straight-chain starch due to hydrophobic forces to form a stable structure, and thus deconvolution of MPS-LOA required higher temperature conditions. Type II structures exhibit high-temperature resistance and good thermal stability (Guo et al., 2021), which can also effectively prevent water and enzyme molecules from entering the interior of starch, which can be blocked in the exterior, and reduce the availability of binding sites in starch (Raza et al., 2021), which is conducive to improving the indigestibility of MPS-LOA. The XRD and NMR results of this study also indicate that MPS-LOA is structurally resistant to digestion and enzymatic digestion. Chen et al. (2018) prepared lotus seed starch-mono stearic acid glycerol complexes using a high-pressure homogenization method and found that the characteristic thermal structure of the starch changed from type I to type II, with a higher melting point and thermal stability. Moreover, the ΔH of MPS-LOA was found to be higher than that of MPS at 8.95 J/g, which can be attributed to the destruction of the structure of MPS-LOA due to distortion of the crystalline region of MPS granules during microwave preparation, dissociation of the double helix structure of the granules, alteration of the accessibility of water molecules to the starch granules, and formation of a more ordered and structurally stable helical structure due to cooled recrystallization (Huang et al., 2021). Lee et al. (2021) prepared debranched wheat starch-saturated FA complexes using a water bath method and found that in DSC analysis, both ΔH and the helical structure content of the complexes increased, showing a type II crystal structure. This finding is consistent with the results of the present study. Zhang et al. (2022) also found that the increased ΔH of pea starch-FA complexes with a stable and ordered crystal structure reduced the hydrolysis rate of starch and increased resistance to digestion, leading to a lower blood insulin response.

Absolute molecular weight analysis

The results of the absolute molecular weight determination for MPS and MPS-LOA are shown in Fig. 5. As shown in the figure, the addition of LOA caused *P*1, which represents branched chain starch, to decrease and shift to the right, and *P*2, which represents straight chain starch with a small molecular weight, to increase and shift to the left. This indicates that the α-1,6 bond of millet starch is hydrolyzed during debranching and microwave preparation, and that the long-branched starch chain is cut off and converted to a large number of medium- and short, straight-chain fragments with short-branched starch (Liu et al., 2020, Lee et al., 2021), thus increasing the small molecular weight fraction. The tight structure of the original starch was broken, and the reactive group was dissolved, which contributed to complexation with LOA. The heavy mean molecular weight (Mw), number mean molecular weight (Mn), and root mean square radius (Rn) of MPS-LOA decreased compared to MPS, with Mw decreasing from 3.16×10^4 kDa to 2.20×10^4 kDa and Rn decreasing from 115.1 nm to 107.1 nm, but the polydispersity index increased from 1.83 to 2.18, indicating that MPS-LOA exhibits general polydispersity (Guo et al., 2019). During the complexation of MPS with LOA, the starch macromolecules and glycosidic bonds are broken, the helical structure is deconvoluted, the amorphous and crystalline regions are destroyed, complex recrystallization reactions occur, the structure is

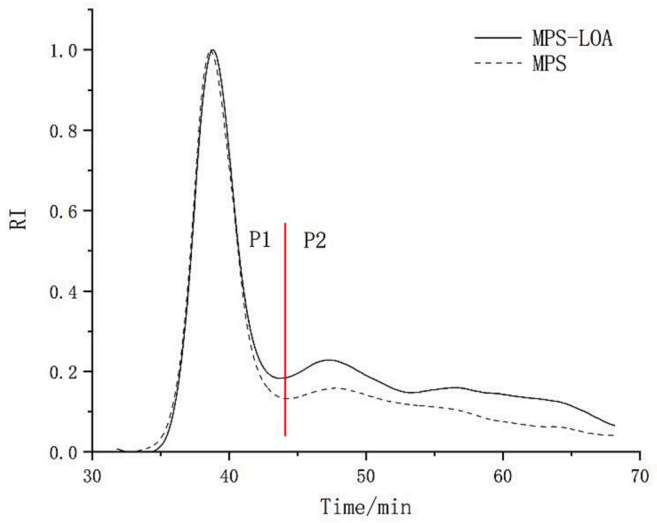

Fig. 5. Molecular size distribution curves of MPS and MPS-LOA.

rearranged, smaller molecular weight glucan aggregates are formed, and the absolute molecular weight of starch decreases (Kang et al., 2022). Additionally, as MPS-LOA is a low-molecular-weight molecule, its mobility is increased, intermolecular forces are enhanced, and the rearranged structure becomes denser, which effectively hinders the entry of digestive enzymes (Chen et al., 2018), making MPS-LOA more resistant to digestion (Li et al., 2021).

Conclusions

In this study, we investigated the structural characteristics, physicochemical properties, and in-vitro hypoglycemic regulatory mechanisms of amylose-FA complex RS of debranched millet. The experiments showed that the MPS-LOA complex prepared using the microwave method had the highest RS content of 40.35 %, which was higher than that of the other five types of starch-FA complexes prepared under the same conditions. As the FA content of MPS-LOA increased, the red fluorescence chromogenic reaction intensified, the UV characteristic peaks moved to lower wavelengths, a color reduction effect appeared, new peaks and functional groups such as C═O appeared at 2853 cm^{-1} and 1400 cm^{-1}, the natural crystalline structure disappeared completely, and V-shaped crystals with high crystallinity were formed. The single helix structure was uniformly distributed and highly ordered, and the absolute molecular weight decreased. MPS-LOA shifted to a more thermally and structurally stable and digestion-resistant type II structure, with decreased swelling power, increased coagulability, inhibitory effects on α-glucosidase, and significantly increased inhibition of α-amylase. Moreover, MPS-LOA significantly reduced the hydrolysis rate of starch by in-vitro hydrolysis kinetic analysis, with a significantly lower eGI and stronger anti-digestive ability, which can be applied as a low eGI product and can be added to hypoglycemic drugs and functional foods, providing a new direction for the exploration of its in-vitro hypoglycemic potential.

Institutional review board statement

Not applicable.

Informed consent statement

Not applicable.

CRediT authorship contribution statement

Yunfei Ge: Conceptualization, Methodology, Investigation, Software, Writing – original draft. **Yu Shi:** Methodology, Formal analysis, Investigation, Software. **Yunjiao Wu:** Conceptualization, Methodology, Validation, Investigation, Data curation. **Chunhong Wei:** Formal analysis, Investigation, Writing – review & editing. **LongKui Cao:** Writing – review & editing, Resources, Funding acquisition.

Declaration of Competing Interest

The authors declare that they have no known competing financial interests or personal relationships that could have appeared to influence the work reported in this paper.

Data availability

Data will be made available on request.

Acknowledgments

This work was supported by the National Key R&D Program of China (2021YFD2100902), the Technology Major Program of Heilongjiang Province of Department of Science and Technology (2021ZX12B06).

Appendix A. Supplementary data

Supplementary data to this article can be found online at https://doi.org/10.1016/j.fochx.2023.100929.

References

Bangar, S. P. S. A. K., Nehra, M., et al. (2021). Structural and Film-Forming Properties of Millet Starches: A Comparative Study. *Coatings, 11*(8), 954.
Cervantes-Ramirez, J. E., Cabrera-Ramirez, A. H., Morales-Sanchez, E., Rodriguez-Garcia, M. E., Reyes-Vega, M. L., Ramirez-Jimenez, A. K., et al. (2020). Amylose-lipid complex formation from extruded maize starch mixed with fatty acids. *Carbohydrate Polymer., 246*, Article 116555.
Chen, B., Guo, Z., Zeng, S., Tian, Y., Miao, S., & Zheng, B. (2018). Paste structure and rheological properties of lotus seed starch-glycerin monostearate complexes formed by high-pressure homogenization. *Food Research International, 103*, 380–389.
Chumsri, P., Panpipat, W., Cheong, L. Z., & Chaijan, M. (2022). Formation of intermediate amylose rice starch–lipid complex assisted by ultrasonication. *Foods, 11*, 2430.
Dang, N. H., Nhung, P. H., Mai Anh, B. T., Thu Thuy, D. T., Minh, C. V., & Dat, N. T. (2016). Chemical composition and α-glucosidase inhibitory activity of Vietnamese citrus peels essential oils. *Journal of Chemistry., 2016*, 1–5.
Englyst, H. N. K. S. M., & Cummings, J. H. (1992). Classification and measurement of nutritionally important starch fractions. *European Journal of Clinical Nutrition, 46*, S33–S50.
Govindaraju, I., Zhuo, G. Y., Chakraborty, I., Melanthota, S. K., Mal, S. S., Sarmah, B., et al. (2022). Investigation of structural and physico-chemical properties of rice starch with varied amylose content: A combined microscopy, spectroscopy, and thermal study. *Food Hydrocolloids, 107093*.
Granfeldt, Y., Björck, I., Drews, A., & Tovar, J. (1994). An in vitro procedure based on chewing to predict metabolic response to starch in cereal and legume products. *European Journal of Clinical Nutrition., 59*, 777S–S.
Guo, T., Hou, H., Liu, Y., Chen, L., & Zheng, B. (2021). In vitro digestibility and structural control of rice starch-unsaturated fatty acid complexes by high-pressure homogenization. *Carbohydrate Polymer., 256*, Article 117607.
Guo, Z., Jia, X., Lin, X., Chen, B., Sun, S., & Zheng, B. (2019). Insight into the formation, structure and digestibility of lotus seed amylose-fatty acid complexes prepared by high hydrostatic pressure. *Food and Chemical Toxicology., 128*, 81–88.
Gutiérrez, T. J., & Tovar, J. (2021). Update of the concept of type 5 resistant starch (RS5): Self-assembled starch V-type complexes. *Trends in Food Science & Technology, 109*, 711–724.
Huang, L., Li, S., Tan, C. P., Feng, Y., Zhang, B., Fu, X., et al. (2021). Solid encapsulation of lauric acid into "empty" V-type starch: Structural characteristics and emulsifying properties. *Carbohydrate Polymer, 267*, Article 118181.
Jenkins, D. J., Wolever, T., Taylor, R. H., Barker, H., Fielden, H., Baldwin, J. M., et al. (1981). Goff D.V. Glycemic index of foods: A physiological basis for carbohydrate exchange. *The American Journal of Clinical Nutrition, 34*, 362–366.
Jia, X., Sun, S., Chen, B., Zheng, B., & Guo, Z. (2018). Understanding the crystal structure of lotus seed amylose–long-chain fatty acid complexes prepared by high hydrostatic pressure. *Food Research International, 111*, 334–341.
Kang, X., Liu, P., Gao, W., Wu, Z., Yu, B., Wang, R., et al. (2020). Sun C. Preparation of starch-lipid complex by ultrasonication and its film forming capacity. *Food Hydrocolloids, 99*.
Krishnan, V., Mondal, D., Bollinedi, H., Srivastava, S., Ramesh, S., Madhavan, L., et al. (2020). Cooking fat types alter the inherent glycaemic response of niche rice varieties through resistant starch (RS) formation. *International Journal of Biological Macromolecules., 162*, 1668–1681.
Le-Bail, P., Houinsou-Houssou, B., Kosta, M., Pontoire, B., Gore, E., & Le-Bail, A. (2015). Molecular encapsulation of linoleic and linolenic acids by amylose using

hydrothermal and high-pressure treatments. *Food Research International, 67*, 223–229.
Lee, M. H., Kim, H. R., Lim, W. S., Kang, M. C., Choi, H. D., & Hong, J. S. (2021). Formation of debranched wheat starch-fatty acid inclusion complexes using saturated fatty acids with different chain length. *LWT – Food Science and Technology., 141*.
Liu, J., Fei, L., Maladen, M., Hamaker, B. R., & Zhang, G. (2009). Iodine binding property of a ternary complex consisting of starch, protein, and free fatty acids. *Carbohydrate Polymer, 75*, 351–355.
Liu, P., Fang, Y., Zhang, X., Zou, F., Gao, W., Zhao, H., et al. (2020). Effects of multienzyme treatment on the physicochemical properties of maize starch-lauric acid complex. *Food Hydrocolloids, 107*.
Liu, S., Sun, S., Chen, W., Jia, R., Zheng, B., & Guo, Z. (2022). Structural, physicochemical properties, and digestibility of lotus seed starch-conjugated linoleic acid complexes. *International Journal of Biological Macromolecules, 214*, 601–609.
Li, X., Gao, X., Lu, J., Mao, X., Wang, Y., Feng, D., et al. (2019). Complex formation, physicochemical properties of different concentration of palmitic acid yam (Dioscorea pposita Thunb.) starch preparation mixtures. *LWT - Food Science and Technology, 101*, 130–137.
Ma, Z., Yin, X., Hu, X., Li, X., Liu, L., & Boye, J. I. (2018). Structural characterization of resistant starch isolated from Laird lentils (Lens culinaris) seeds subjected to different processing treatments. *Food Chemistry, 263*, 163–170.
Millan-Testa, C. E., Mendez-Montealvo, M. G., Ottenhof, M. A., Farhat, I. A., & Bello-Pérez, L. A. (2005). Determination of the Molecular and Structural Characteristics of Okenia, Mango, and Banana Starches. *Journal of Agricultural and Food Chemistry, 53*, 495–501.
Muthamilarasan, M., & Prasad, M. (2021). Small millets for enduring food security amidst pandemics. *Trends in Plant Science, 26*, 33–40.
Oskaybas-Emlek, B., Ozbey, A., Aydemir, L. Y., & Kahraman, K. (2022). Production of buckwheat starch-myristic acid complexes and effect of reaction conditions on the physicochemical properties, X-ray pattern and FT-IR spectra. *International Journal of Biological Macromolecules, 207*, 978–989.
Oyeyinka, S. A., Singh, S., & Amonsou, E. O. (2021). A review on structural, digestibility and physicochemical properties of legume starch-lipid complexes. *Food Chemistry, 349*, Article 129165.
Raza, H., Ameer, K., Ren, X., Liang, Q., Chen, X., Chen, H., et al. (2021). Physicochemical properties and digestion mechanism of starch-linoleic acid complex induced by multi-frequency power ultrasound. *Food Chemistry, 364*, Article 130392.
Sangilimuthu, A. Y., Sivaraman, T., Chandrasekaran, R., Sundaram, K. M., & Ekambaram, G. (2021). Screening chemical inhibitors for alpha-amylase from leaves extracts of Murraya koenigii (Linn.) and Aegle marmelos L. *Journal of Complementary and Integrative Medicine, 18*, 51–57.
Tan, I., Flanagan, B. M., Halley, P. J., Whittaker, A. K., & Gidley, M. J. (2007). A method for estimating the nature and relative proportions of amorphous, single, and double-helical components in starch granules by 13C CP/MAS NMR. *Biomacromolecules, 8*, 885–891.
Tao, Y., Yan, B., Fan, D., Zhang, N., Ma, S., Wang, L., et al. (2020). Structural changes of starch subjected to microwave heating: A review from the perspective of dielectric properties. *Trends in Food Science & Technology, 99*, 593–607.
Van, H. P., Lan, P. N. T., & Vy, T. T. (2012). Effect of debranching and storage condition on crystallinity and functional properties of cassava and potato starches. *Starch – Stärke, 64*, 964–971.
Wang, H., Wang, J., Liu, Y., Ji, Y., Guo, Y., & Zhao, J. (2019). Interaction mechanism of carnosic acid against glycosidase (α-amylase and α-glucosidase). *International Journal of Biological Macromolecules, 138*, 846–853.
Wang, J., Li, Y., Tian, Y., Xu, X., Ji, X., Cao, X., et al. (2010). A novel triple-wavelength colorimetric method for measuring amylose and amylopectin contents. *Starch-Stärke, 62*, 508–516.
Wu, F., Chi, B., Xu, R., Liao, H., Xu, X., & Tan, X. (2022). Changes in structures and digestibility of amylose-oleic acid complexes following microwave heat-moisture treatment. *International Journal of Biological Macromolecules, 214*, 439–445.
Xu, X., Chen, Y., Luo, Z., & Lu, X. (2019). Different variations in structures of A-and B-type starches subjected to microwave treatment and their relationships with digestibility. *LWT - Food Science and Technology, 99*, 179–187.
Zhang, X., Mi, T., Gao, W., Wu, Z., Yuan, C., Cui, B., et al. (2022). Ultrasonication effects on physicochemical properties of starch-lipid complex. *Food Chemistry, 388*, Article 133054.